

1 The instrument constant of sky radiometers (POM-02),

2 Part II: Solid view angle

3
4 Akihiro Uchiyama¹, Tsuneo Matsunaga¹, Akihiro Yamazaki²

5
6 ¹ Center for Global Environmental Research, National Institute for Environmental
7 Studies, Tsukuba, Ibaraki 305-8506, Japan

8 ² Meteorological Research Institute, Japan Meteorological Agency, Tsukuba, Ibaraki
9 305-0052, Japan

10 *Correspondence to:* Uchiyama Akihiro (uchiyama.akihiro@nies.go.jp)

11
12
13 **Abstract**

14 Ground-based networks have been developed to determine the spatiotemporal
15 distribution of aerosols using sky radiometers. In this study, errors related to the solid
16 view angle (SVA) of sky radiometers, which are used by SKYNET, were investigated.
17 The SVA is calculated using solar disk scan data, the measured radiances around the
18 solar direction in 0.1×0.1 degree increments. These measurements include the
19 scattered light from aerosol and air molecules, as well as the direct solar irradiance,
20 causing errors in the SVA calculation. The influence of these errors was evaluated with
21 simulations. From the results of these simulations, if the aerosol optical **depth (optical**
22 **path length)** is less than 0.5 (0.58) at 550 nm and the aerosol does not include large
23 particles, such as desert dust particles, then its influence on the SVA calculation was
24 less than 0.5%. Problems with the software for the SVA calculation were also
25 investigated. First, the data processing does not consider the change of airmass (solar
26 zenith angle) during the solar disk scan measurement. In practice, if a measurement is
27 made in the period when the change in airmass is small, then the error is small.
28 Second, before starting data processing, the minimum measured value is subtracted
29 from the measured values, resulting in underestimation of the SVA by 1 to 4%. Thirdly,
30 the values between 1.4 and 2.5 degrees are not properly extrapolated, resulting in

31 overestimation of the SVA by 0.6 to 2.1%. The second and third error sources partially
32 cancel each other out, and the total error is an underestimation of 0.5 to 1.9% of the
33 actual value. Furthermore, the annual trend in the SVA was examined. In both the
34 visible and near-infrared regions (Si photodiode region) and in the shortwave-infrared
35 region (InGaAs photodiode region), this trend cannot be seen in 4 and 8 years of data,
36 respectively. The seasonal variation of the SVA was also examined, but no clear
37 seasonal variation could be detected.

38

39 1. Introduction

40 Atmospheric aerosols are an important constituent of the atmosphere. Aerosols
41 affect not only the global climate through the radiation budget both directly and
42 indirectly (e.g., Ramanathan et al. 2001, Lohmann and Feichter 2005) but also human
43 health as one of the main components of air pollution.

44 Atmospheric aerosols have a large variability in time and space. To measure the
45 spatiotemporal distribution of aerosols, ground-based observation networks such as
46 AERONET (AErosol RObotic NETwork) (Holben et al. 1998) and SKYNET (Takamura
47 and Nakajima 2004) have been developed and extended, and remote sensing methods
48 from space have been developed using the near-ultraviolet to shortwave-infrared
49 wavelengths.

50 For ground-based observations, the solar direct irradiance and sky radiances are
51 measured, and the aerosol characteristics are retrieved by analyzing these data. To
52 improve the measurement accuracy, it is important to know the characteristics of the
53 instrument and to be able to accurately calibrate it.

54 In SKYNET, radiometers POM-01 and POM-02 manufactured by Prede Co. Ltd.,
55 Japan are used. These radiometers are called ‘sky radiometers’, and measure both the
56 solar direct irradiance and sky radiances. The objectives in this study are to
57 investigate the current status and issues with sky radiometers.

58 There are two constants that we must determine to be able to make accurate
59 measurements. One is the calibration constant. The other is the solid view angle (SVA)
60 of the radiometer. In Part I (Uchiyama et al. 2018), the temperature dependence of the
61 sensor output was investigated and the calibration constants determined by the
62 Improved Langley method and normal Langley method were compared. An alternative
63 method to determine the calibration constant for the 940 nm channel and the
64 shortwave-infrared channels (1225, 1627, 2200 nm) was shown using on-site
65 measurement data.

66 In Part II, the problem related to the SVA of the sky radiometer is described. The

67 SVA connects the sensor output to the sky radiance, which has units of
 68 energy/(wavelength)/sr. Overestimation (underestimation) in the SVA leads to
 69 underestimation (overestimation) of the single-scattering albedo (SSA). Therefore, it is
 70 necessary to accurately determine the SVA (Khatri et al. 2016, Hashimoto et al. 2012).

71 In section 2, the accuracy of the current method for the SVA calculation is
 72 investigated based on simulations. Then, in section 3, we describe the problem with the
 73 current SVA calculation program. This software is attached to the SKYRAD package
 74 (Nakajima et al. 1996), which is used to retrieve aerosol parameters from sky
 75 radiometer data. In section 4, we also show the trend in the SVA and seasonal
 76 variation using the data obtained at MLO and JMA/MRI. In section 5, the results and
 77 conclusions are presented.

78

79 **2. Simulation study of SVA estimation error**

80 The sensor output V when measuring the radiances from the sky with a sky
 81 radiometer can be written as follows:

$$82 \quad V = \int_{\Delta} C(\lambda_0) f(\Omega) I(\Omega) d\Omega \quad (1)$$

$$\quad = C(\lambda_0) \bar{I} \Delta\Omega$$

83 where C is the sensitivity, $I(\Omega)$ is the sky radiance in the direction of Ω , $f(\Omega)$ is
 84 the response function of the radiometer field of view,

$$85 \quad \bar{I} = \int_{\Delta} f(\Omega) I(\Omega) d\Omega / \Delta\Omega \quad (2)$$

$$86 \quad \Delta\Omega = \int_{\Delta} f(\Omega) d\Omega \quad (3)$$

87 and, for simplicity, the wavelength integration is omitted. Here, $\Delta\Omega$ is the SVA,
 88 which is related to the mean sky radiance in the direction of Ω , and errors in the SVA
 89 result in errors in the retrieved SSA. Therefore, the SVA is an important instrument
 90 parameter.

91 The SVA can be obtained by integrating the output of parallel light incident on the
 92 radiometer from all directions (see Appendix A). The SVA can also be obtained even if
 93 the light source has a finite size: the SVA can be obtained by integrating the output
 94 obtained while scanning the light source (see Appendix B).

95 To determine the SVA, a method using the measurement data around the sun was
 96 proposed by Nakajima et al. (1996). The radiances around the direction of the sun in
 97 0.1×0.1 degree increments are measured; this is called a “solar disk scan”. Using
 98 these data, the SVA is calculated. [Using similar gridded data, Torres et al. \(2013\)](#)

99 calculated the SVA of the Cimel-318 Sun-photometer and compared it with the values
100 obtained by other methods.

101 An example of measurements of the radiance of the sun and around the sun is shown
102 in Fig. 1. The measurements at POM-02 were performed vertically at intervals in the
103 scattering angle of 0.1 degrees, where the wavelengths are 380, 500, and 675 nm. Here,
104 “vertically” means that the measurements were performed while keeping the azimuth
105 angle the same as the solar azimuth angle. In Fig. 1, the values are normalized by the
106 measured value at the zero scattering angle (the direct solar irradiance), where a
107 positive (negative) value means a higher (lower) solar elevation. At any wavelength,
108 the output of POM-02 changes greatly around the scattering angles of -2.5 and 2.5
109 degrees. This means that the output of POM-02 is affected by the direct solar
110 irradiance for up to about ± 2.5 degrees from the sun direction.

111 The hood of POM-02 is designed so that the full field of view (FOV) is 1 degree. The
112 size of the sun disk is about 0.5 degrees. Therefore, the direct solar irradiance can
113 enter the detector for angles up to about 0.75 degrees from the sun’s center. For ideal
114 instruments, the output outside about 0.75 degrees should be the output due to light
115 scattered by air molecules and atmospheric aerosols. However, Fig. 1 shows that the
116 sensor output of POM-02 is affected by the direct solar irradiance for angles up to
117 about ± 2.5 degrees from the sun’s center.

118 The cause of the increase in the output between 0.75 and 2.5 degrees is considered to
119 be stray light. Since the length of the hood and the size of the lens are finite, even if the
120 angle from the sun center exceeds 0.75 degrees, the direct solar light strikes the lens
121 and results in “stray” light. This stray light reaches the detector and increases the
122 output, and is smaller than the measurement of the direct sun by three orders of
123 magnitude or more, but the integrated value has a magnitude that can affect the
124 estimation of the SVA. Furthermore, when solar light is used as the light source,
125 aerosols and air molecules exist between the light source and the instrument.
126 Therefore, the scattered light from aerosols and air molecules is included in the
127 measurement of the direct solar irradiance. The influence of this scattered light must
128 also be considered.

129 As seen from Fig. 1, roughly speaking, the FOV of POM-02 consists of a core part
130 from 0 to 0.5 degrees and a wing part from 0.5 to 2.5 degrees.

$$\begin{aligned} \Delta\Omega &= \Delta\Omega(\text{core}) + \Delta\Omega(\text{wing}) \\ &= \int_{\Delta\Omega(\text{core})} f(\Omega)d\Omega + \int_{\Delta\Omega(\text{wing})} f(\Omega)d\Omega \end{aligned} \quad (3)$$

132 Estimating the magnitudes of the two terms gives the following:

$$\begin{aligned}
\Delta\Omega(core) &= \int_{\Delta\Omega(core)} f(\Omega)d\Omega \\
133 \quad &\cong \int_{\Delta\Omega(core)} 1 \cdot d\Omega \\
&= 2\pi(1 - \cos(0.5 \text{ deg})) \\
&= 2.39 \times 10^{-4}
\end{aligned} \tag{4}$$

$$\begin{aligned}
\Delta\Omega(wing) &= \int_{\Delta\Omega(wing)} f(\Omega)d\Omega \\
134 \quad &\cong \int_{\Delta\Omega(wing)} f_{wing} d\Omega \\
&= 2\pi(\cos(0.5 \text{ deg}) - \cos(2.5 \text{ deg}))f_{wing} \\
&= 5.74 \times 10^{-3} f_{wing}
\end{aligned} \tag{5}$$

135 As seen from Fig. 1, $f_{wing} \approx 10^{-3}$. Therefore, the ratio of the terms is

$$136 \quad \frac{\Delta\Omega(wing)}{\Delta\Omega(core)} \approx \frac{5.74 \times 10^{-3} f_{wing}}{2.39 \times 10^{-4}} = 2.4 \times 10^{-2}. \tag{6}$$

137 This means that neglecting the wing part results in underestimation of the magnitude
138 of the SVA by about 2%. If $f_{wing} \approx 10^{-2}$, then the contribution of the wing part to the
139 SVA is about 20%, and the instrument should be repaired. If $f_{wing} \approx 10^{-4}$, then the
140 contribution is about 0.2%, and the wing part can be ignored. [The magnitude of the
141 sensor output between 0.75 and 2.5 degrees depends on the internal structure of the
142 skyradiometer and the optical constant of the material.](#)

143 When the direction of the sun is measured, the sensor output $V(\Omega = 0)$ is as follows:

$$\begin{aligned}
144 \quad V(\Omega = 0) &= C \left[\int_{\Delta} f(\Omega') I_0 g(\Omega') d\Omega' + \int_{\Delta\Omega} I_{sca}(\Omega') f(\Omega') d\Omega' \right] \\
&= v(0) + C\Delta\Omega \bar{I}_{sca}(0)
\end{aligned} \tag{7}$$

145 where

$$146 \quad v(0) = C \int_{\Delta} f(\Omega') I_0 g(\Omega') d\Omega' \tag{8}$$

$$147 \quad \bar{I}_{sca}(0) = \frac{1}{\Delta\Omega} \int_{\Delta\Omega} I_{sca}(\Omega') f(\Omega') d\Omega' \tag{9}$$

148 and $I_0 g(\Omega')$ is the solar radiance distribution. The first term on the right-hand side

149 of eq. (7) is the contribution of the direct solar irradiance, and the second term is that
 150 of the scattered radiance.

151 When the direction of the sun is $\Omega = \Omega_0$, the sensor output $V(\Omega = \Omega_0)$ is as
 152 follows:

$$153 \quad V(\Omega = \Omega_0) = C \left[\int_{\Delta} f(\Omega_0 + \Omega') I_0 g(\Omega') d\Omega' + \int_{\Delta\Omega} I_{sca}(\Omega_0 + \Omega') f(\Omega') d\Omega' \right] \quad (10)$$

$$= v(\Omega_0) + C\Delta\Omega \bar{I}_{sca}(\Omega_0)$$

154 where the first term on the right-hand side is the contribution of the direct solar
 155 irradiance, and the second term is the scattered radiance. If Ω_0 is outside of the field
 156 of view, then the first term is zero and only the second term is needed.

157 Currently, based on the data of the solar disk scan measurement, the SVA is
 158 calculated by the following equation:

$$159 \quad \Delta\Omega' = \int_{\Delta\Omega} \frac{v(\Omega) + \Delta\Omega C \bar{I}_{sca}(\Omega)}{v(0) + \Delta\Omega C \bar{I}_{sca}(0)} d\Omega \quad (11)$$

160 If there is no scattered radiance, then

$$161 \quad \Delta\Omega' = \int_{\Delta\Omega} \frac{v(\Omega)}{v(0)} d\Omega \quad (12)$$

162 where $\Delta\Omega'$ is the SVA $\Delta\Omega$ (see Appendices A, B).

163 If the contribution of the scattered radiance is small, then $\Delta\Omega' \cong \Delta\Omega$. When the
 164 optical [depth](#) is large or the forward scattering is dominant, the contribution of the
 165 scattered radiances increases.

166 We estimate the magnitude of each term of the integrand:

$$167 \quad \frac{v(\Omega) + \Delta\Omega C \bar{I}_{sca}(\Omega)}{v(0) + \Delta\Omega C \bar{I}_{sca}(0)} = \frac{v(\Omega) + \Delta\Omega C \bar{I}_{sca}(\Omega)}{v(0)(1 + \Delta\Omega C \bar{I}_{sca}(0)/v(0))} \quad (13)$$

168 Usually, the solar disk scan measurement is performed only when the scattered light is
 169 much less than the direct solar irradiance:

$$170 \quad \Delta\Omega C \bar{I}_{sca}(0)/v(0) \ll 1.$$

171 The magnitude of this term has already been estimated from the influence of the
 172 scattered radiance in the field of view in the measurement of the sun-photometer; the
 173 estimation error of the optical [depth](#) due to the scattered radiance in the field of view
 174 (Zhao et al. 2012, Sinyuk et al. 2012).

175 Equation (13) can be approximated as follows:

$$\begin{aligned}
\frac{\nu(\Omega) + \Delta\Omega C\bar{I}_{sca}(\Omega)}{\nu(0) + \Delta\Omega C\bar{I}_{sca}(0)} &\cong \frac{\nu(\Omega) + \Delta\Omega C\bar{I}_{sca}(\Omega)}{\nu(0)} \left(1 - \frac{\Delta\Omega C\bar{I}_{sca}(0)}{\nu(0)}\right) \\
176 \quad &= \frac{\nu(\Omega) + \Delta\Omega C\bar{I}_{sca}(\Omega)}{\nu(0)} (1 - \varepsilon_3) \\
&= \frac{\nu(\Omega)}{\nu(0)} + \frac{\Delta\Omega C\bar{I}_{sca}(\Omega)}{\nu(0)} - \frac{\nu(\Omega)}{\nu(0)} \varepsilon_3 - \frac{\Delta\Omega C\bar{I}_{sca}(\Omega)}{\nu(0)} \varepsilon_3
\end{aligned} \tag{14}$$

177 where

$$178 \quad \varepsilon_3 = \frac{\Delta\Omega C\bar{I}_{sca}(0)}{\nu(0)}. \tag{15}$$

179 Therefore, eq. (11) is as follows:

$$\begin{aligned}
\Delta\Omega' &= \int_{\Delta\Omega} \frac{\nu(\Omega) + \Delta\Omega C\bar{I}_{sca}(\Omega)}{\nu(0) + \Delta\Omega C\bar{I}_{sca}(0)} d\Omega \\
180 \quad &\cong \Delta\Omega + \Delta\Omega \int_{\Delta\Omega} \frac{C\bar{I}_{sca}(\Omega)}{\nu(0)} d\Omega - \Delta\Omega \varepsilon_3 - \Delta\Omega \int_{\Delta\Omega} \frac{C\bar{I}_{sca}(\Omega)}{\nu(0)} d\Omega \varepsilon_3 \\
&= \Delta\Omega \left\{ 1 + \int_{\Delta\Omega} \frac{C\bar{I}_{sca}(\Omega)}{\nu(0)} d\Omega - \varepsilon_3 - \varepsilon_3 \int_{\Delta\Omega} \frac{C\bar{I}_{sca}(\Omega)}{\nu(0)} d\Omega \right\}
\end{aligned} \tag{16}$$

181 Since $\nu(0) = CF_0$, where F_0 is the solar irradiance at the top of the atmosphere,
182 and C is the proportional constant (sensitivity) (see Appendix B), the above eq. (16)
183 becomes

$$\begin{aligned}
184 \quad \Delta\Omega' &\cong \Delta\Omega \left\{ 1 + \int_{\Delta\Omega} \frac{\bar{I}_{sca}(\Omega)}{F_0} d\Omega - \varepsilon_3 - \varepsilon_3 \int_{\Delta\Omega} \frac{\bar{I}_{sca}(\Omega)}{F_0} d\Omega \right\} \\
&= \Delta\Omega \{ 1 + \varepsilon_2 - \varepsilon_3 - \varepsilon_2 \varepsilon_3 \}
\end{aligned} \tag{17}$$

185 in which

$$186 \quad \varepsilon_2 = \int_{\Delta\Omega} \frac{\bar{I}_{sca}(\Omega)}{F_0} d\Omega \tag{18}$$

187 The fourth term is smaller than the second and third terms and it can be ignored. Then,
188 comparing the second and third terms in the curly brackets,

$$189 \quad \varepsilon_2 = \int_{\Delta\Omega} \frac{\bar{I}_{sca}(\Omega)}{F_0} d\Omega = \int_{\Delta\Omega} \left\{ \frac{1}{F_0} \cdot \frac{1}{\Delta\Omega} \int_{\Delta\Omega} I_{sca}(\Omega + \Omega') f(\Omega') d\Omega' \right\} d\Omega \tag{19}$$

$$\begin{aligned}
\varepsilon_3 &= \frac{\Delta\Omega}{F_0} \cdot \frac{1}{\Delta\Omega} \int_{\Delta\Omega} I_{sca}(0 + \Omega') f(\Omega') d\Omega' \\
190 \quad &= \frac{\Delta\Omega \bar{I}_{sca}(\Omega = 0)}{F_0}
\end{aligned} \tag{20}$$

191 where ε_2 is the integral of the mean scattered light $\bar{I}_{sca}(\Omega)$ in the region of
 192 $f(\Omega) > 0$, and ε_3 is the integral of scatted light in the FOV when facing toward the
 193 sun.

194 The $f(\Omega)$ of the POM-02 consists of the core part from 0.0 to 0.5 degrees, which
 195 takes large values, and the wing part from 0.5 to 2.5 degrees which takes small values.
 196 Therefore, the integral can be written as follows:

$$197 \quad \varepsilon_2 = \int_{\Delta\Omega} \frac{\bar{I}_{sca}(\Omega)}{F_0} d\Omega = \int_{\Delta\Omega(core)} \frac{\bar{I}_{sca}(\Omega)}{F_0} d\Omega + \int_{\Delta\Omega(wing)} \frac{\bar{I}_{sca}(\Omega)}{F_0} d\Omega \quad (21)$$

198 Since $\bar{I}_{sca}(\Omega) \approx \bar{I}_{sca}(\Omega = 0)$ in the core part, $\int_{\Delta\Omega(wing)} f(\Omega) d\Omega \ll 1$, and $\int_{\Delta\Omega(core)} d\Omega \cong \Delta\Omega$,

199 the first term of the integral ε_2 is as follows:

$$200 \quad \int_{\Delta\Omega(core)} \frac{\bar{I}_{sca}(\Omega)}{F_0} d\Omega \cong \frac{\bar{I}_{sca}(\Omega = 0)}{F_0} \Delta\Omega. \quad (22)$$

201 This means that the integral of the core part in the integral ε_2 has the same
 202 magnitude as ε_3 and the two terms offset each other, whereas the integral of the wing
 203 part remains. The area of the integral of the wing part is larger than that of the core
 204 part. Even if the integral of scattered light in the FOV is small compared to the solar
 205 direct irradiance, the integral of the wing part becomes large and introduces errors in
 206 the SVA estimation. That is, even if the measurement value of scattered light is
 207 smaller than the direct sun measurement, $\bar{I}_{sca}(\Omega)\Delta\Omega/F_0 \approx 10^{-3}$, the integral of the
 208 wing part becomes large:

$$209 \quad \int_{\Delta\Omega(wing)} \frac{\bar{I}_{sca}(\Omega)}{F_0} d\Omega \approx \frac{\Delta\Omega(wing)}{\Delta\Omega} \times 10^{-3} \approx \frac{\Delta\Omega(wing)}{\Delta\Omega(core)} \times 10^{-3} = 2.4 \times 10^{-2}. \quad (23)$$

210 In this case, the magnitude of the error is about 2%.

211 Figures 2 and 3 show the values of ε_2 and ε_3 when the aerosol optical [depth](#) at
 212 550 nm is changed. Here, the solar zenith angle is 30 degrees and the aerosol models
 213 are the OPAC Continental average, Urban, and Desert types (Hess et al. 1998). The
 214 simulation calculations of the scattered sky radiances were performed using the
 215 subroutine in the SKYRAD package. The Ångström exponents of the Continental
 216 average in the shorter (350 to 500 nm) and longer (500 to 800 nm) wavelength regions

217 are 1.11 and 1.42, respectively. Those of the Urban areas are 1.14 and 1.43, respectively,
218 and those of the Desert are 0.20 and 0.17, respectively.

219 When comparing ε_2 and ε_3 , the signs are opposite and partially cancel out.

220 However, ε_3 is one order of magnitude smaller than ε_2 , and thus ε_2 contributes to
221 the error in the calculation of the SVA. In the Continental average and Urban models,
222 if the aerosol optical depth (optical path length = optical depth \times airmass) at 550 nm is
223 less than 0.5 ($0.50/\cos(30^\circ) = 0.58$), then the second term ε_2 is less than 0.5%, and if
224 the aerosol optical depth at 550 nm is less than 1, then the second term ε_2 is less than
225 1%. In the Desert model, which includes large particles, the second term is less than
226 1% for shorter wavelengths, where desert particles have a higher absorption than in
227 the longer wavelength regions. However, even if the aerosol optical depth at 550 nm is
228 less than 0.5, the second term is larger than 1% for some wavelengths.

229 From these simulations, if the scattered light can be removed from the SVA
230 calculation, then an improvement in the accuracy of the calculations can be expected.
231 However, since the intensity of the scattered light depends on aerosol characteristics, it
232 is difficult to estimate the intensity of the scattered light from the measurements.
233 Furthermore, close to the sun, the value of scattered light cannot be measured due to
234 the direct sunlight. In POM-01 and POM-02, scattered light can only be measured
235 without being affected by direct sunlight at scattering angles of more than 3 degrees.

236 The SVA was calculated by subtracting the measurements for a scattering angle of 3
237 degrees and the accuracy of the estimation was examined. Although not shown in
238 detail, for the continental average and urban models, even if the aerosol optical depth
239 (optical path length) is 2 (2.3) at 550 nm, the error in the SVA estimation was less than
240 0.5%. This indicates that if the measured value of scattered light can be subtracted, the
241 estimation accuracy of the SVA can be greatly improved.

242 From these results, when we determine the SVA by using the data from the solar
243 disk scan measurement, if the aerosol optical depth (optical path length) is less than
244 0.5 (0.58) and the aerosol does not include large particles such as desert dust particles,
245 the effect of the scattered radiances on the SVA calculation is less than 0.5%, and $\Delta\Omega$
246 is well approximated by $\Delta\Omega'$. Furthermore, if the measured value of the scattered
247 light can be subtracted, the estimation accuracy of SVA can be greatly improved.

248

249 3. SVA calculation with the SKYRAD package

250 The software in the SKYRAD package (Nakajima et al. 1996) is often used for SVA

251 calculation from the data of the solar disk scan measurement. However, the authors
252 noticed that there are problems in this program, and this section investigates these
253 problems in detail. In Appendix C, a flowchart is shown illustrating the SVA
254 calculation procedure in the SKYRAD package.

255 In the measurement of the solar disk scan, a range of ± 1 degree in the zenith angle
256 direction and ± 1 degree in the azimuth direction relative to the sun in increments of
257 0.1 degrees is used, which produces a 21×21 grid with an angular resolution of 0.1
258 degrees. Therefore, the data are taken from the sun for scattering angles of up to about
259 $1.4 (= (1 \text{ degree}) \times \sqrt{2})$ degrees. As shown in Fig. 1, the influence of the direct solar
260 irradiance as a light source extends to about 2.5 degrees. To take this into
261 consideration, the integration is performed by extrapolation for angles larger than 1.4
262 degrees.

263 The following three problems exist in the SKYRAD package for calculating the SVA.

264 First, the data processing does not consider changes in the airmass (solar zenith
265 angle) during the solar disk scan measurement. However, in practice, if the solar disk
266 scan measurement is conducted when the airmass change (solar zenith angle) is small,
267 then the resulting error is also small. Also, this is not usually a problem unless the
268 measurement is conducted over an extended period of time.

269 Second, before starting the data processing, the minimum measured value is
270 subtracted from the measured values. As a result, the measurements of the scattering
271 angle between 1 and 1.4 degrees are greatly affected. By integrating the measured
272 value minus the minimum, the SVA is always underestimated, but the solution to this
273 problem is not straightforward.

274 Thirdly, the values between 1.4 and 2.5 degrees are not properly extrapolated.
275 Frequently, the extrapolated value does not decrease monotonically. In some cases, this
276 partially cancels out the underestimation of the integral.

277 In Fig. 4, an example of the integrand for the SVA calculation is shown. In the blue
278 curve with open squares, the minimum value is subtracted. This curve is then
279 integrated by the current SKYRAD program. Since the minimum value is subtracted,
280 the difference is noticeable at scattering angles greater than 1 degree. In this case, the
281 extrapolated value from 1.4 to 2.5 degrees is almost constant. In many cases, nearly
282 constant values were extrapolated as in this example. In some cases, the extrapolated
283 values increased. In the red curve with open circles, the minimum value is not
284 subtracted. The values between 1.4 and 2.5 degrees were extrapolated using the data
285 from 1.0 to 1.4 degrees. Considering Fig. 1, the decreasing trend is more realistic.

286 Furthermore, Manago et al (2016) showed, using lamp-based measurements at the
287 ground level, that the FOV monotonically decreases to around 2.5 degrees and then
288 sharply decreases as the scattering angle increases.

289 To investigate the differences in the calculation methods, several calculations were
290 performed.

291 The following steps in the calculations were varied:

- 292 (1) Whether the minimum value was subtracted.
- 293 (2) Whether the change in airmass was considered.
- 294 (3) The method for the extrapolation in the range from 1.4 to 2.5 degrees.
- 295 (4) Whether the horizontal cross-section of the FOV is assumed to be a circle or an
296 ellipse (the current SKYRAD package method uses an ellipse).
- 297 (5) The method for determining the ellipse's parameters.

298 Data taken at MLO in October and November in 2015 were used in this study.
299 The solar disk scan measurement was made between 10:00 and 13:00 local time at
300 MLO. The optical depth at wavelengths of 500 and 340 nm were at most 0.1 and 0.5,
301 respectively. Therefore, the influence of the scattered light on the SVA calculation is
302 small.

303 The SAV was calculated for the six cases shown in Table 1, including Case 1, which is
304 the current method used by the SKYRAD package. In Cases 4, 5, and 6, the values in
305 the range 1.4 to 2.5 degrees were extrapolated as a linear function of the cosine of the
306 scattering angle. This linear function was determined by the least squares method
307 using the data with a scattering angle of more than 1 degree. In Cases 3, 4, 5, and 6,
308 assuming that the aerosol optical depth has not changed, the solar direct irradiance
309 changes due to the change of the airmass during the measurement. The elliptic
310 parameters in Case 6 were determined by assuming that the shape of the FOV is a
311 2-dimensional Gaussian distribution. The results of the comparison are summarized in
312 Table 2.

313 The difference between Case 1 and Case 2 is whether or not the minimum value was
314 subtracted. Case 1, in which the minimum value was subtracted, results in an
315 underestimation of about 1 to 4%.

316 The standard deviation in the region of shorter wavelengths in Case 1 is smaller
317 than for the other cases. One of the causes of the variation of the calculated SVA is the
318 variation of the wing part of the FOV. In the region of shorter wavelengths, generally,
319 the optical depth is thicker than the longer wavelength region, and the scattered light
320 increases in the shorter wavelength region. When the minimum value is subtracted
321 from the measurement value, the value of the wing portion decreases greatly in the

322 shorter wavelength region, and the contribution to the SVA integration also decreases
323 greatly in the short wavelength region. As a result, the variance of the calculated SVA
324 becomes small. However, there is no justification for subtracting the minimum value.

325 The difference between Case 2 and Case 3 is whether the change in airmass was
326 considered or not. The solar disk scan measurement was made between 10:00 and
327 13:00 local time at MLO. Therefore, the change in the air mass is less than 0.01, and
328 there was hardly any influence from the change in airmass.

329 The difference between Case 3 and Case 4 is the method of extrapolation used in the
330 range from 1.4 to 2.5 degrees. In the current SKYRAD package, the SVA was
331 overestimated by 0.6 to 2.1%.

332 Since there was hardly any influence from the change in airmass, in Case 1 and Case
333 4 the underestimation caused by the subtraction of the minimum value and the
334 overestimation caused by the poor extrapolation partially cancel each other out, and
335 the current SKYRAD package method underestimates the SVA by 0.5 to 1.9%.

336 The difference between Case 3 and Case 5 is whether the horizontal cross-section of
337 the FOV is assumed to be a circle or an ellipse. The difference between them was less
338 than 0.1%. This indicates that POM-02 was well tuned when it was shipped from the
339 manufacturer.

340 In Case 6, a different method for determining elliptic parameters from the current
341 SKYRAD package was used. Therefore, the difference between Case 4 and Case 6 is
342 the difference between the methods used to determine the elliptic parameters. There
343 was almost no difference between the current method and the new method. The
344 method used to determine the elliptic parameters thus has little effect on the SVA
345 estimation.

346

347 **4. Annual trend and seasonal variation of SVA**

348 Broadly speaking, the SVA is determined by the size of the pinhole and the focal
349 length of the lens. There is a possibility that these parameters may change with
350 degradation and the inside temperature. Therefore, the annual trend and seasonal
351 variation of the SVA are examined.

352 Figures 5 and 6 show the SVAs in the visible and near-infrared region (Si
353 photodiode) and in the shortwave-infrared region (InGaAs photodiode) for 2008 and
354 2016, respectively. The observation for the calibration at MLO was performed over
355 about a month in October and November each year. The lens in the visible region was
356 replaced before the observation in 2013.

357 In Fig. 5(a), time series of the SVA in channels 1 to 8 (from 340 nm to 1020 nm) are

358 shown for the SVA calculated by the corrected method in this study. In Fig. 5(b), the
359 SVA in channel 4 (500 nm) calculated by both the corrected and the current SKYRAD
360 package methods are shown for comparison. As stated in the above section, the SVA
361 calculated by the current method is lower than that calculated by the corrected one
362 except for 2008. Since the lens in the visible and near-infrared region was replaced
363 before the calibration observation in 2013, it is difficult to investigate the annual trend
364 of the SVA. Additionally, from this figure, the uncertainty of the SVA (standard
365 deviation/mean) is estimated at about 1% except in 2015.

366 From 2008 to 2012, the value of the SVA seems to be decreasing. The value of the
367 SVA in 2008 is larger than in other years. The mean values of the SVA are within
368 $\pm 0.5\%$ except in 2008. From 2013 to 2016, the mean values of the SVA are within $\pm 1\%$.
369 The annual variation of the SVA is less than or equal to the uncertainty of the SVA.
370 From these results, the annual trend in the SVA cannot be seen in only 4 years of data,
371 and even if there is a trend, it is smaller than the measurement uncertainty.

372 Figure 6(a) is the same as Fig. 5(a) except for channels 9 to 11 (1225, 1627, 2200 nm)
373 and Fig. 6(b) is the same as Fig. 5(b) except for channel 10 (1627 nm). In these
374 channels, the SVA calculated by the current method is also lower than that calculated
375 by the corrected one except in 2008.

376 The determination uncertainty of the SVA is also estimated as about 1%. The lens in
377 the shortwave-infrared region was not replaced in the period from 2008 to 2016. The
378 trend in the SVA cannot be seen in 8 years of data either. The values of the SVA in this
379 period are within $\pm 1\%$, which is the determination uncertainty of the SVA. From these
380 results, the annual trend of the SVA in the shortwave-infrared channels cannot be seen
381 in 8 years of data, and even if there is a trend, it is smaller than the measurement
382 uncertainty.

383 Figure 7 shows the SVAs of POM-02 (Tsukuba) in the 500 and 1627 nm channels in
384 the period from January 2014 to December 2016. All data are plotted and the data are
385 scattered about ± 1.5 and $\pm 2\%$ (standard deviation/mean), though the values in 2014
386 are a bit low. There is a large amount of data in the winter, because there are many
387 fine days in the winter in Tsukuba. There are little data from spring to autumn and the
388 data in the summer are scattered. Since the estimated SVA is scattered, it is not
389 possible to draw a clear conclusion, but as can be seen from Fig. 7, the seasonal
390 variation exceeding $\pm 2\%$ cannot be confirmed in either channel. This also indicates
391 that the temperature dependence of the SVA in both detector regions cannot be seen.
392 Since the data are taken over a short period of 3 years, no annual trend in the SVA can
393 be detected.

394

395 **5. Summary and conclusion**

396 Atmospheric aerosols are an important constituent of the atmosphere. Measurement
397 networks covering an extensive area from ground and space have been developed.
398 SKYNET is a ground-based monitoring system using sky radiometers POM-01 and
399 POM-02 (Prede Co. Ltd., Japan). To improve the measurement accuracy, it is
400 important to know the characteristics of the instruments and calibrate them. There
401 are two constants that we must determine to make accurate measurements. One is the
402 calibration constant, and the other is the SVA of the radiometer.

403 In Part I, problems related to the estimation of the calibration constant were
404 investigated, and in Part II, problems related to the determination of the SVA of the
405 sky radiometer were described.

406 In this study, the data from two sky radiometers POM-02 of the JMA/MRI **were**
407 analyzed. One of the sky radiometers **was** used as a calibration reference, and the
408 other **was** used for the continuous measurement at the Tsukuba MRI observation site.

409 The FOV of POM-02 consists of a core part from 0 to 0.5 degrees and a wing part
410 from 0.5 to 2.5 degrees. The wing part is about 3 orders of magnitude smaller than the
411 core part, but the wing part contributes about 2% to the SVA.

412 A method for determining the SVA using the sun as a light source was proposed by
413 Nakajima et al. (1996). In this method, the radiance around the direction of the sun in
414 0.1×0.1 degree increments is measured. These measurements include the scattered
415 light from aerosols and air molecules as well as the direct solar irradiance. These
416 scattered radiances cause errors in the SVA calculation.

417 The influence of the scattered light was evaluated by simulations. As a result, if the
418 aerosol optical **depth (optical path length)** is less than 0.5 (**0.58**) at a wavelength of 550
419 nm and the aerosol does not include large particles such as desert dust particles, then
420 the effect of the scattered radiances on the SVA calculation is less than 0.5%.
421 Furthermore, if the measurements of the scattered light can be taken into account, the
422 estimation accuracy of the SVA can be greatly improved.

423 The SKYRAD package for determining the SVA from the solar disk scan
424 measurements has several problems. The problems do not result in major errors in the
425 estimation of the SVA, but can cause a systematic underestimation.

426 First, the data processing does not consider the change in the airmass (solar zenith
427 angle) during the solar disk scan measurement. In practice, if the measurements are
428 taken over a period when the change in airmass is small, then there is almost no
429 problem. Second, before beginning the data processing, the minimum value is

430 subtracted from each measured value. This results in an underestimation of the SVA
431 by 1 to 4%. Thirdly, the values between 1.4 and 2.5 degrees are not properly
432 extrapolated. This overestimates the SVA value by 0.6 to 2.1%. Since the second and
433 third errors partially cancel each other out, if the current software is used, the overall
434 error will be an underestimation by 0.5 to 1.9%.

435 The annual trend in the SVA was examined using the data taken at MLO. Since the
436 optical depth at a wavelength of 500 nm is 0.1 at most at MLO, the influence of the
437 scattered light is small. The uncertainty of the SVA was estimated as about 1%. In the
438 visible and near-infrared region, the annual trend in the SVA could not be seen in only
439 4 years of data from 2009 to 2012 and 2013 to 2016, and it was smaller than the
440 measurement accuracy. In the shortwave-infrared region, the annual trend of the SVA
441 could not be seen in 8 years data from 2008 to 2016, and it was smaller than the
442 measurement uncertainty.

443 The seasonal variation of the SVA was examined using the data taken at Tsukuba
444 from January 2014 to December 2016. Since the time series of the determined SVA was
445 scattered over a range of $\pm 2\%$, it is not possible to draw a clear conclusion, but seasonal
446 variation exceeding $\pm 2\%$ could not be confirmed. Furthermore, as the temporal range
447 of the data was short, no annual trend could be detected.

448 According to the method based on the current measurement data, the uncertainty is
449 1% at high-altitude mountain sites such as MLO and 1.5 to 2% at low-altitude sites
450 such as Tsukuba. The cause of the error may be an increase in the scattered light in the
451 optically thick case, a variation in the solar direct irradiance due to a change in the
452 aerosol concentration during the solar disk scan measurement, and an error in the
453 pointing direction of the FOV. In the future, we will eliminate scattered light and use
454 measurements of the aerosol optical depth by other instruments during the solar disk
455 scan measurement. We will also develop methods for measuring the SVA on the ground
456 or in a laboratory.

457 **Acknowledgements**

458 This work was supported by the NIES GOSAT-2 project, Japan. This work was also
459 partially supported by JSPS KAKENHI Grant Number JP17K00531.

460

461

462 **Appendix A**

463 Let $f(\Omega)$ be the response function of the FOV, where Ω indicates the direction,
464 and when $\Omega = 0$, $f(\Omega = 0) = 1$.

465 The SVA is then as follows:

466
$$\Delta\Omega = \int_{\Delta} f(\Omega)d\Omega . \tag{A1}$$

467 Suppose parallel light enters from $\Omega = \Omega_0$.

468
$$\begin{aligned} V(\Omega = \Omega_0) \\ &= C \int_{\Delta} f(\Omega)\delta(\Omega - \Omega_0)F_0 d\Omega \\ &= Cf(\Omega = \Omega_0)F_0 \end{aligned} \tag{A2}$$

469 Here, F_0 is the input irradiance, and C is the proportional constant (sensitivity).

470 Therefore,

471
$$f(\Omega_0) = \frac{V(\Omega_0)}{CF_0} . \tag{A3}$$

472 Since $f(0) = 1$, then $V(0) = CF_0$.

473 Therefore,

474
$$\begin{aligned} \Delta\Omega &= \int_{\Delta} f(\Omega)d\Omega \\ &= \int_{\Delta} \frac{V(\Omega_0)}{CF_0} d\Omega_0 \\ &= \int_{\Delta} \frac{V(\Omega_0)}{V(0)} d\Omega_0 \end{aligned} \tag{A4}$$

475 When the parallel light is incident, the SVA of the radiometer can be obtained by
476 integrating the output in an arbitrary direction normalized by the output in the
477 direction of $\Omega = 0$.

478

479 **Appendix B**

480 Here, we consider the case that the light source has a finite size, for example, when
481 the sun is used as a light source.

482 Let the radiance distribution of the light source be $I(\Omega) = I_0g(\Omega)$.

483 The integrated energy of the light source F_0 is as follows:

484
$$F_0 = \int_{\Delta} g(\Omega)I_0d\Omega \tag{B1}$$

485 where Δ is the extent of the light source.

486 Considering the sun as a light source, let Δ be smaller than $\Delta\Omega$. Also, when the
487 sun is a light source, F_0 is the solar irradiance.

488 Let C be the sensitivity of the detector, where C is the proportional constant of
489 the sensor output and input energy.

490 The light source is in the direction of $\Omega = 0$ and we measure the radiance from it as

$$\begin{aligned}
v(0) &= C \int_{\Delta} f(0 + \Omega') g(\Omega') I_0 d\Omega' \\
&= CI_0 \int_{\Delta} f(\Omega') g(\Omega') d\Omega'
\end{aligned} \tag{B2}$$

where $v(0)$ is the sensor output.

If $f(\Omega)$ is constant within the range of Δ (POM-02 satisfies this condition), then this equation can be rewritten as follows:

$$\begin{aligned}
v(0) &= CI_0 \int_{\Delta} f(\Omega') g(\Omega') d\Omega' \\
&= CI_0 f(0) \int_{\Delta} g(\Omega') d\Omega' \\
&= Cf(0)F_0 \\
&= CF_0
\end{aligned} \tag{B3}$$

Next, the light source is in the direction of $\Omega = \Omega_0$:

$$v(\Omega_0) = CI_0 \int_{\Delta} f(\Omega_0 + \Omega') g(\Omega') d\Omega' \tag{B4}$$

where $v(\Omega_0)$ is the sensor output.

Then, both sides of the equation are integrated within the SVA $\Delta\Omega$:

$$\int_{\Delta\Omega} v(\Omega_0) d\Omega_0 = \int_{\Delta\Omega} \left(CI_0 \int_{\Delta} f(\Omega_0 + \Omega') g(\Omega') d\Omega' \right) d\Omega_0 \tag{B5}$$

By changing the order of integration on the right, the following equation can be obtained:

$$\begin{aligned}
\int_{\Delta\Omega} v(\Omega_0) d\Omega_0 &= CI_0 \int_{\Delta} \left(g(\Omega') \int_{\Delta\Omega} f(\Omega_0 + \Omega') d\Omega_0 \right) d\Omega' \\
&= CI_0 \int_{\Delta} g(\Omega') d\Omega' \cdot \Delta\Omega \\
&= CF_0 \Delta\Omega
\end{aligned} \tag{B6}$$

Therefore, from eqs. (B3) and (B6),

$$\begin{aligned}
\Delta\Omega &= \frac{1}{CF_0} \int_{\Delta\Omega} v(\Omega_0) d\Omega_0 \\
&= \int_{\Delta\Omega} \frac{v(\Omega_0)}{v(0)} d\Omega_0
\end{aligned} \tag{B7}$$

Thus, even in the case that the light source has a finite size, the SVA of the radiometer can be obtained in the same manner as in the case of the parallel light source.

509

510 [Appendix C](#)

511 [In Fig. C1, a flowchart is shown of the SVA calculation procedure in the SKYRAD](#)
512 [package.](#)

513

514 **References**

- 515 Hashimoto M., T. Nakajima, O. Dubovik, M. Campanelli, H. Che, P. Khatri, T.
516 Takamura, and G. Pandithurai, 2012: Development of a new data-processing method
517 for SKYNET sky radiometer observations, *Atmos. Meas. Tech.*, **5**, 2723–2737, 2012,
518 www.atmos-meas-tech.net/5/2723/2012/doi:10.5194/amt-5-2723-2012
- 519 Hess, M., P. Koepke, and I. Schult, Optical Properties of Aerosols and Clouds, 1998:
520 The Software Package OPAC. *Bull. Am. Meteorol. Soc.*, **79**, 5, 831-844.
- 521 Holben, B. N., T. F. Eck, I. Slutsker, D. Tanré, J. P. Buis, A. Setzer, E. Vermote, J. A.
522 Reagan, Y. J. Kaufman, T. Nakajima, F. Lavenu, I. Jankowiak, and A. Smirnov, 1998:
523 AERONET-A federated instrument network and data archive for aerosol
524 characterization. *Remote Sens. Environ.*, **66**, 1-16.
- 525 P. Khatri, P., T. Takamura, T. Nakajima, V. Estellés, H. Irie, H. Kuze, M. Campanelli, A.
526 Sinyuk, S.-M. Lee, B. J. Sohn, G. Pandithurai, S.-W. Kim, S. C. Yoon, J. A.
527 Martinez-Lozano, M. Hashimoto, P. C. S. Devara, and N. Manago, 2016: Factors for
528 inconsistent aerosol single scattering albedo between SKYNET and AERONET, *J.*
529 *Geophys. Res. Atmos.*, **121**, 1859–1877, doi:10.1002/2015JD023976.
- 530 Lohmann, U., and J. Feichter, 2005: Global indirect aerosol effects: a review. *Atmos.*
531 *Chem. Phys.*, **5**, 715-737.
- 532 [Manago, N, K. Pradeep, H. Irie, T. Takamura, and H. Kuze, 2016: On the method of](#)
533 [solid view angle calibration for SKYNET skyradiometers, 4th International](#)
534 [SKYNET workshop, Rome, March 2-4, 2016.](#)
- 535 Nakajima, T., G. Tonna, R. Rao, Y. Kaufman, and B. Holben, 1996: Use of sky
536 brightness measurements from ground for remote sensing of particulate
537 polydispersions, *Appl. Opt.*, **35**, 2672–2686.
- 538 Ramanathan, V., P. J. Crutzen, J. T. Kiehl, and D. Rosenfeld, 2001: Aerosols, Climate,
539 and the Hydrological Cycle. *Science*, **294**, 2119-2124.
- 540 Sinyuk, A., B. N. Holben, A. Smirnov, T. F. Eck, I. Slutsker, J. S. Schafer, D. M. Giles,
541 and M. Sorokin, 2012: Assessment of error in aerosol optical depth measured by
542 AERONET due to aerosol forward scattering, *Geophys. Res. Lett.*, **39**, L23806,
543 doi:10.1029/2012GL053894.
- 544 Takamura, T, T. Nakajima and SKYNET community group, 2004: Overview of

545 SKYNET and its Activities. Proceedings of AERONET workshop. *El Arenosillo.*
546 *Optica Pura y Aplicada*, **37**, 3303–3308.

547 Torres, B., C. Toledano, A. Berjón, D. Fuertes, V. Molina, R. Gonzalez, M. Canini, V. E.
548 Cachorro, P. Goloub, T. Podvin, L. Blarel, O. Dubovik, Y. Bennouna, and A. M. de
549 Frutos, 2013: Measurements on pointing error and field of view of Cimel-318 Sun
550 photometers in the scope of AERONET, *Atmos. Meas. Tech.*, **6**, 2207–2220,
551 doi:10.5194/amt-6-2207-2013.

552 Uchiyama A., T. Matsunaga and A. Yamazki, 2017: The instrument constant of sky
553 radiometers (POM-02), Part I; Calibration constant, *Atmos. Meas. Tech.* (to be
554 submitted)

555 Zhao, F., Y. Tan, Z. Li, and C. Gai ,2012: The effect and correction of aerosol forward
556 scattering on retrieval of aerosol optical depth from Sun photometer measurements,
557 *Geophys. Res. Lett.*, **39**, L14805, doi:10.1029/2012GL052135.

558

559 Table titles

560 Table 1 Settings of the SVA calculation.

561

562 Table 2 Influence of the different calculation settings.

563 (a) Calculated SVA. The data taken at MLO in October and November 2015 are used.

564 (b) Comparison of the calculated SVA.

565

566 Figure captions

567 Fig. 1 An example of measurement of the sun and the sky around the sun. The

568 measurement was performed keeping the same azimuth angle as the solar azimuth

569 angle. A positive (negative) value means a higher (lower) solar elevation, where the

570 wavelengths are 380 nm (red), 500 nm (blue), and 675 nm (green). The values are

571 normalized by the measured value at the zero scattering angle (direct solar

572 irradiance).

573

574 Fig. 2 Estimation of the error ε_2 in the calculation of the SVA. Aerosol models are the

575 OPAC Continental average, Urban, and Desert. The aerosol optical **depth** thickness is

576 that at a wavelength of 550 nm and the solar zenith angle is 30 degrees.

577

578 Fig. 3 Same as Fig. 2 but for error ε_3 .

579

580 Fig. 4 Example of the integrand of the SVA calculation. The blue line with open

581 squares is for the case that the minimum value is subtracted, and the red line is for the

582 case that the values between 1.4 and 2.5 degrees are extrapolated using the data from

583 1.0 to 1.4 degrees.

584

585 Fig. 5 SVAs in the visible **and near-infrared** region (Si photodiode) from 2008 to 2016.

586 The data were taken at MLO over a month in October and November every year. (a)

587 SVA calculated by the corrected method in this study, (b) SVA at a wavelength of 500

588 nm calculated by both the corrected and the current SKYRAD package methods.

589

590 Fig. 6 Same as Fig. 5 but for the **shortwave**-infrared region (InGaAs photodiode). The

591 wavelength in (b) is 1627 nm.

592

593 Fig. 7 Time series of the SVA at POM-02 (Tsukuba) from January 2014 to December

594 2016: (a) 500 nm, the **mean and standard deviation** are 2.743×10^{-4} and 4.2×10^{-6} ,

595 respectively. (b) 1627 nm, the mean and standard deviation are 2.104×10^{-4} and $4.4 \times 10^{-}$
596 6 , respectively.
597

598

599 Table 1 Settings of the SVA calculation.

	Subtract minimum value	Consideration of airmass change	Extrapolation method	FOV shape
Case 1	yes	no	current	elliptic
Case 2	no	no	current	elliptic
Case 3	no	yes	current	elliptic
Case 4	no	yes	new	elliptic
Case 5	no	yes	current	circular
Case 6	no	yes	new	elliptic

600 Case 1 is the method implemented in the current SKYRAD package.

601 [In Case 5, "circular" means that the FOV is axisymmetric.](#)

602 The elliptic shape parameters in Case 6 are calculated by a different method from the
603 SKYRAD package.

604

Table 2 Influence of the different calculation settings.

(a) Calculated SVA. The data taken at MLO in October and November 2015 are used.

WLN (nm)		340	380	400	500	675	870	940	1020	1225	1627	2200
Case_1 (C1)	SVA($\times 10^{-4}$)	2.4495	2.4643	2.4472	2.4366	2.4530	2.4404	2.4554	2.4567	2.0086	2.0152	2.0692
	SD($\times 10^{-4}$)	0.0379	0.0407	0.0403	0.0388	0.0374	0.0277	0.0296	0.0241	0.0287	0.0241	0.0214
	SD/SVA	0.0155	0.0165	0.0165	0.0159	0.0153	0.0113	0.0121	0.0098	0.0143	0.0120	0.0103
Case_2 (C2)	SVA($\times 10^{-4}$)	2.5014	2.5186	2.5036	2.4764	2.4782	2.4995	2.5322	2.5564	2.0586	2.0737	2.1328
	SD($\times 10^{-4}$)	0.1151	0.1116	0.1144	0.0838	0.0579	0.0346	0.0314	0.0257	0.0294	0.0260	0.0233
	SD/SVA	0.0460	0.0443	0.0457	0.0338	0.0234	0.0138	0.0124	0.0101	0.0143	0.0125	0.0109
Case_3 (C3)	SVA($\times 10^{-4}$)	2.5015	2.5184	2.5035	2.4765	2.4783	2.4993	2.5320	2.5565	2.0586	2.0737	2.1327
	SD($\times 10^{-4}$)	0.1151	0.1115	0.1144	0.0838	0.0580	0.0344	0.0315	0.0258	0.0295	0.0260	0.0233
	SD/SVA	0.0460	0.0443	0.0457	0.0338	0.0234	0.0138	0.0124	0.0101	0.0143	0.0125	0.0109
Case_4 (C4)	SVA($\times 10^{-4}$)	2.4693	2.4899	2.4698	2.4534	2.4641	2.4691	2.4923	2.5023	2.0346	2.0440	2.1005
	SD($\times 10^{-4}$)	0.0668	0.0804	0.0698	0.0580	0.0459	0.0304	0.0302	0.0259	0.0301	0.0259	0.0227
	SD/SVA	0.0271	0.0323	0.0283	0.0236	0.0186	0.0123	0.0121	0.0104	0.0148	0.0127	0.0108
Case_5 (C5)	SVA($\times 10^{-4}$)	2.5027	2.5199	2.5032	2.4777	2.4783	2.5010	2.5329	2.5565	2.0596	2.0750	2.1336
	SD($\times 10^{-4}$)	0.1155	0.1123	0.1141	0.0831	0.0583	0.0346	0.0312	0.0262	0.0298	0.0261	0.0236
	SD/SVA	0.0461	0.0446	0.0456	0.0335	0.0235	0.0138	0.0123	0.0102	0.0145	0.0126	0.0111
Case_6 (C6)	SVA($\times 10^{-4}$)	2.4694	2.5042	2.4698	2.4535	2.4637	2.4698	2.4921	2.5028	2.0349	2.0449	2.1014
	SD($\times 10^{-4}$)	0.0669	0.1249	0.0701	0.0576	0.0463	0.0297	0.0305	0.0264	0.0312	0.0258	0.0225
	SD/SVA	0.0271	0.0499	0.0284	0.0235	0.0188	0.0120	0.0122	0.0106	0.0153	0.0126	0.0107
No. of data	19	19	17	20	17	18	17	17	17	20	20	17

(b) Comparison of calculated SVA.

WLN (nm)	340	380	400	500	675	870	940	1020	1225	1627	2200	
C2/C1-1	0.0212	0.0220	0.0230	0.0163	0.0103	0.0242	0.0313	0.0406	0.0249	0.0290	0.0307	min. value subtraction
C3/C2-1	0.0000	-0.0001	0.0000	0.0000	0.0000	-0.0001	-0.0001	0.0000	0.0000	0.0000	0.0000	airmass change
C4/C3-1	-0.0129	-0.0113	-0.0135	-0.0093	-0.0057	-0.0121	-0.0157	-0.0212	-0.0117	-0.0143	-0.0151	different extrapolation
C4/C1-1	0.0081	0.0104	0.0092	0.0069	0.0045	0.0118	0.0150	0.0186	0.0129	0.0143	0.0151	min. value subtraction, different extrapolation
C5/C3-1	0.0005	0.0006	-0.0001	0.0005	0.0000	0.0007	0.0004	0.0000	0.0005	0.0006	0.0004	circular or elliptic shape
C6/C4-1	0.0000	0.0057	0.0000	0.0000	-0.0002	0.0003	-0.0001	0.0002	0.0001	0.0004	0.0004	different elliptic parameters

Fig.1

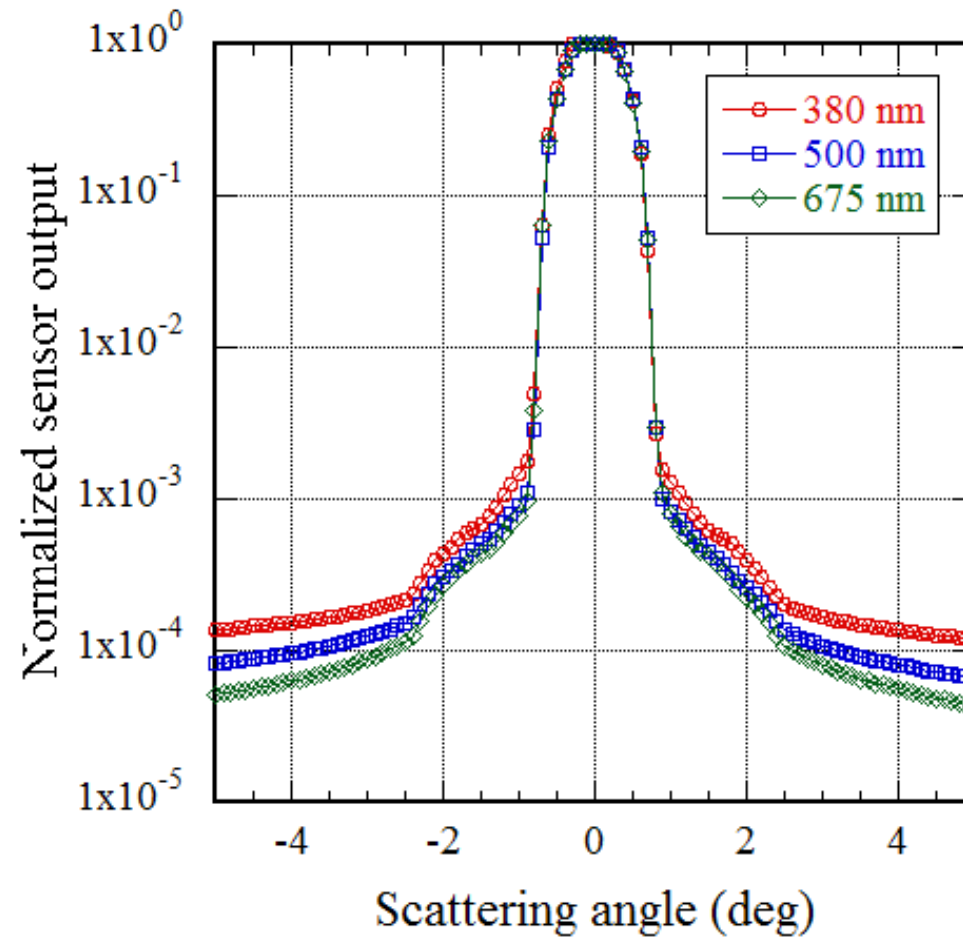
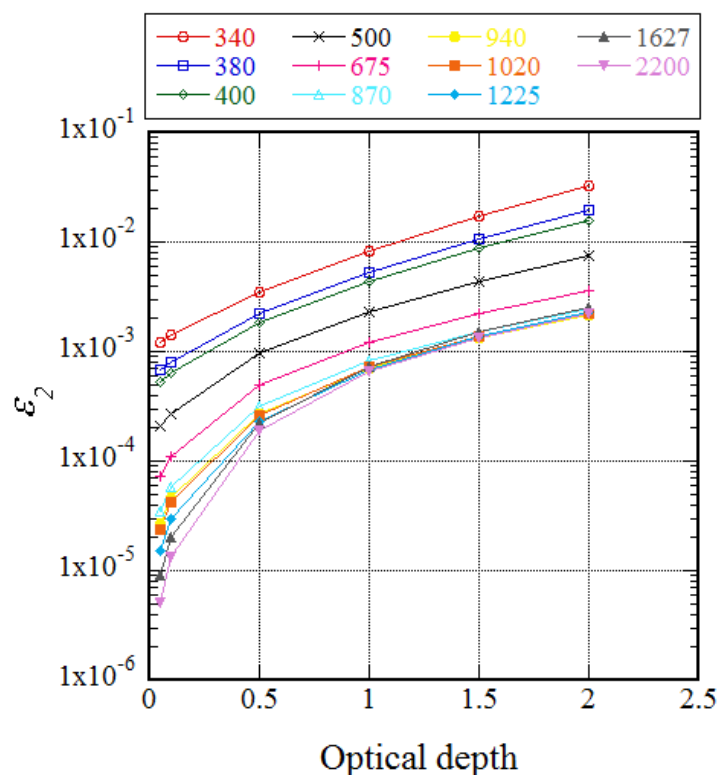


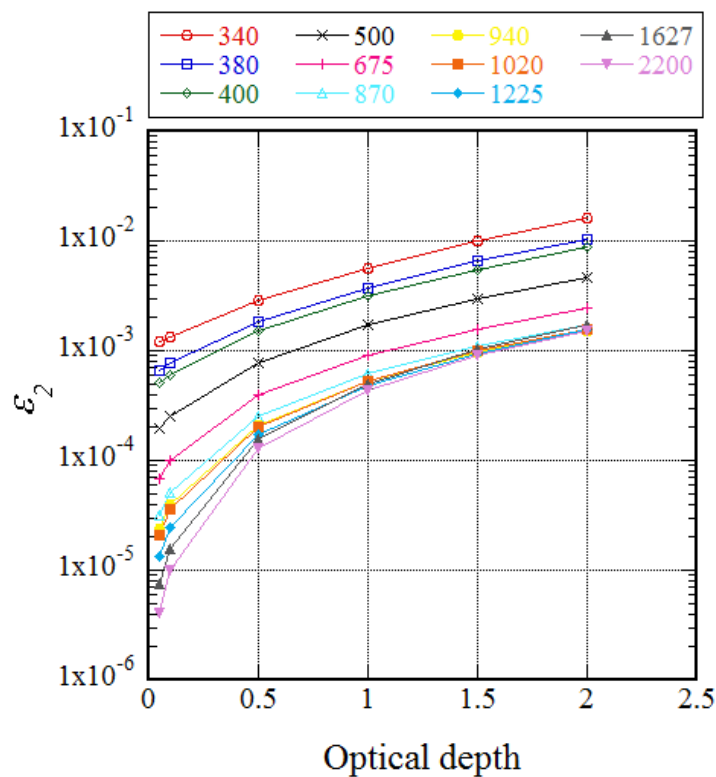
Fig. 1 An example of measurement of the sun and the sky around the sun. The measurement was performed keeping the same azimuth angle as the solar azimuth angle. A positive (negative) value means a higher (lower) solar elevation, where the wavelengths are 380 nm (red), 500 nm (blue), and 675 nm (green). The values are normalized by the measured value at the zero scattering angle (direct solar irradiance).

Fig. 2

(a) Continental average



(b) Urban



(c) Desert

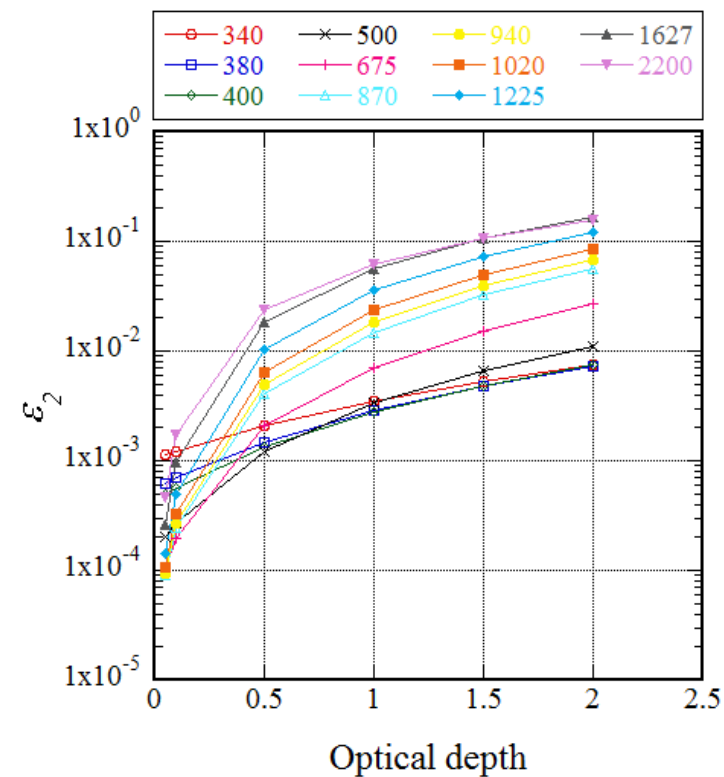


Fig. 2 Estimation of error ε_2 in calculation of SVA. Aerosol models are OPAC continental average, urban and desert. The aerosol optical depth is that at the wavelength of 550nm and the solar zenith angle is 30 deg.

Fig. 3

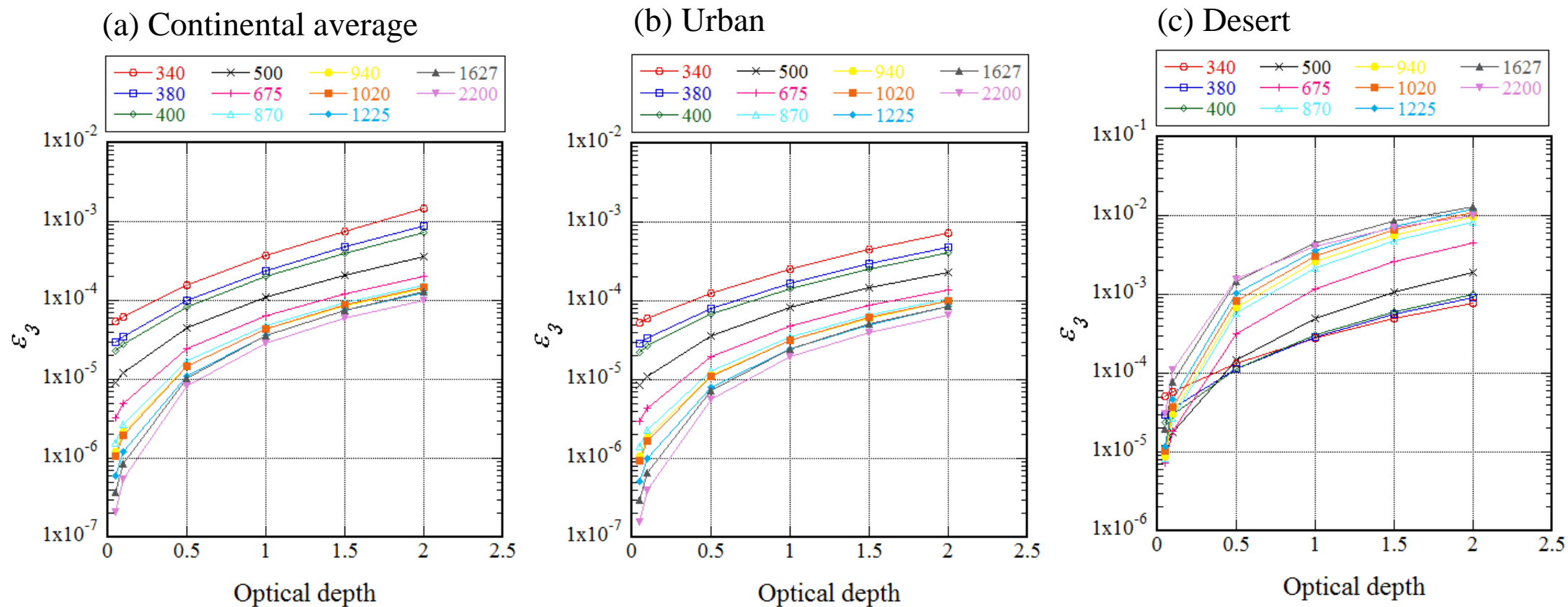


Fig. 3 Same as Fig. 2 but for error ε_3 .

Fig.4

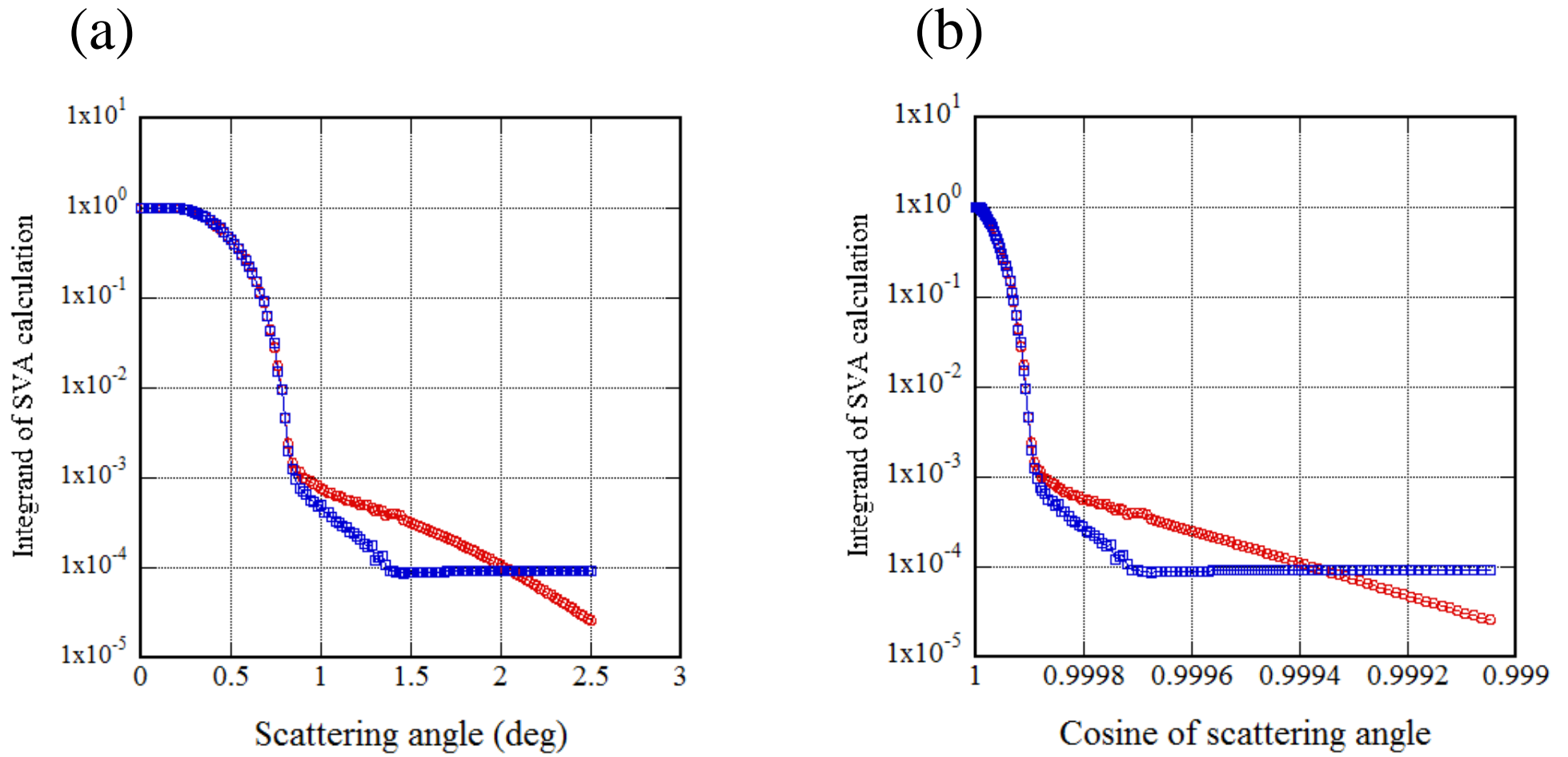


Fig.4 An example of integrand of SVA calculation. The blue line with open squares is the case that the minimum value is subtracted, and the red line is the case that the values between 1.4 and 2.5 degrees are extrapolated using the data from 1.0 to 1.4 degrees

Fig.5

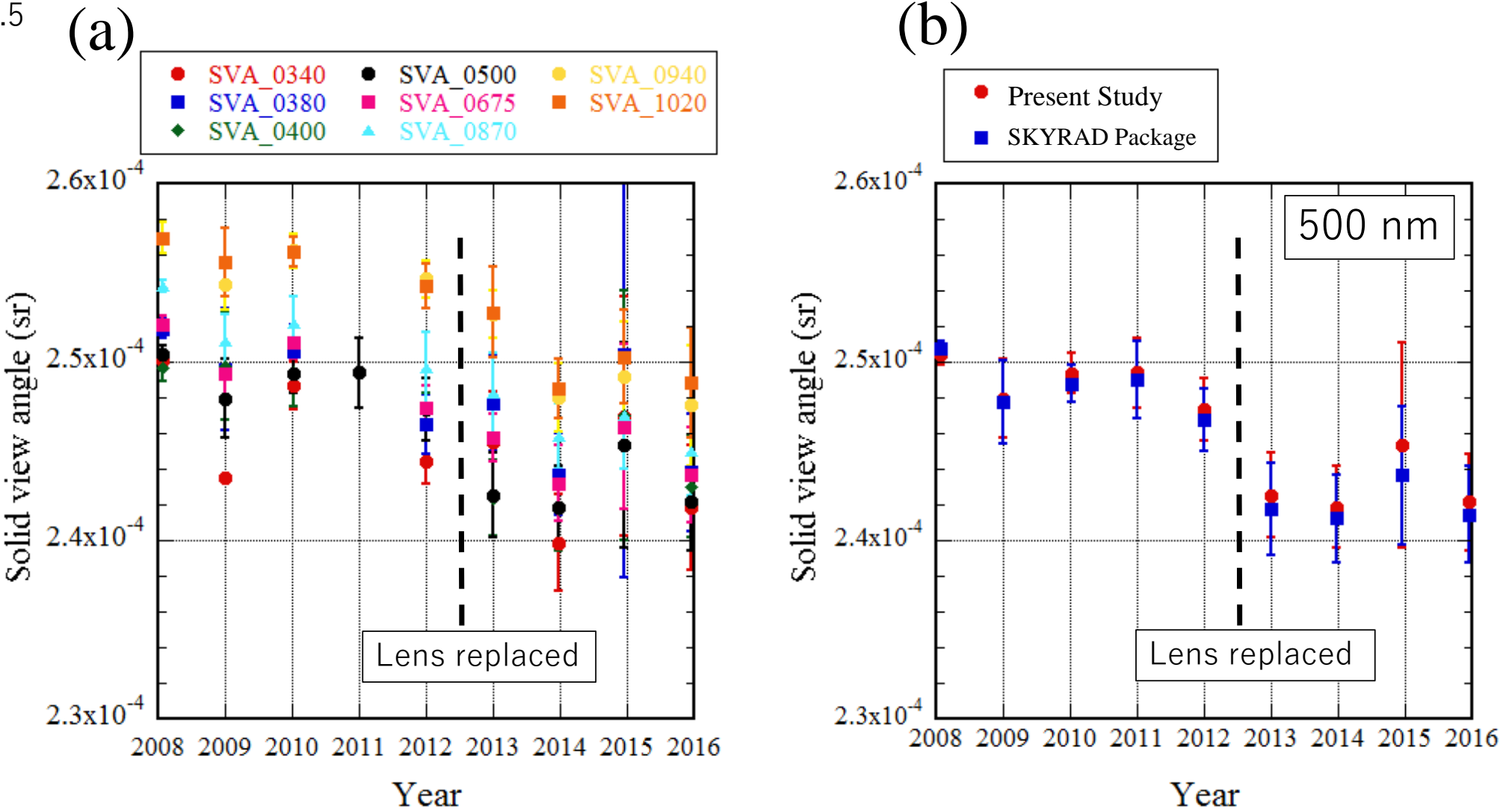
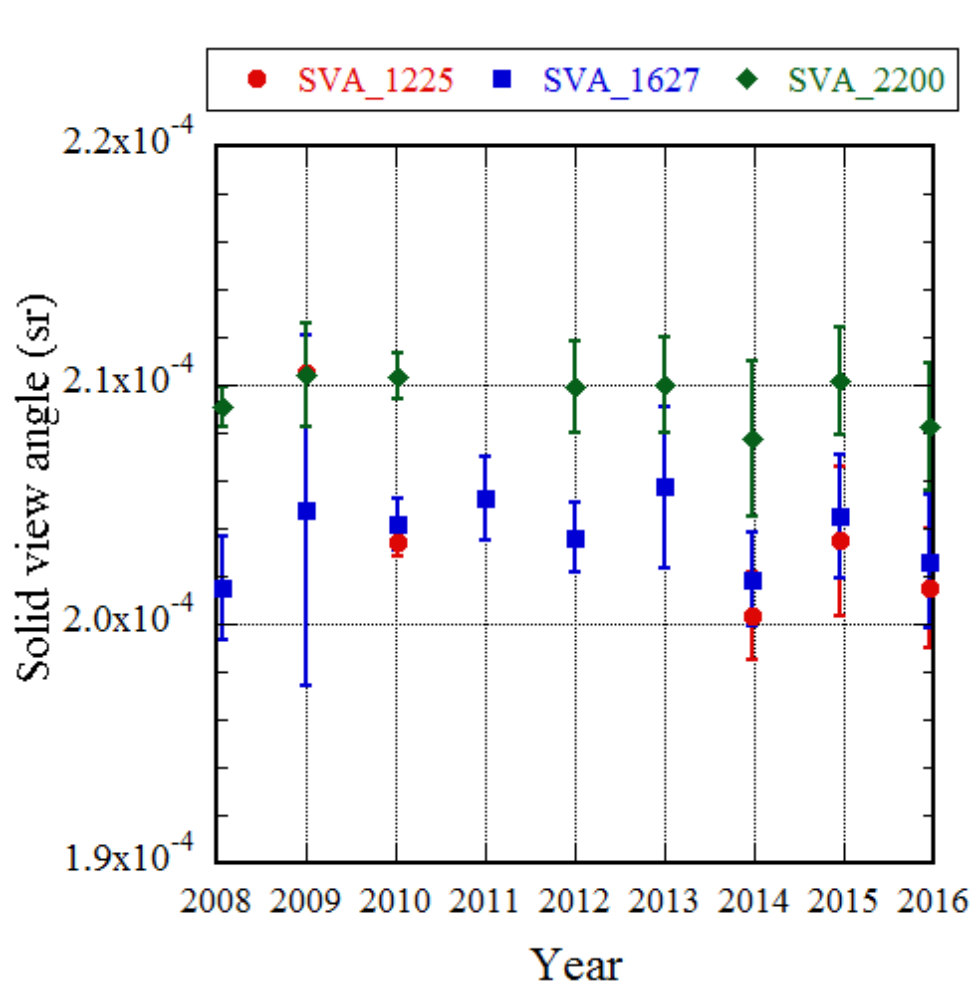


Fig.5 SVAs in the visible and near-infrared region (Si photodiode) from 2008 to 2016. The data were taken at MLO over a month in October and November every year. (a) SVA calculated by the corrected method in this study, (b) SVA at the wavelength of 500 nm calculated by both the corrected and the current SKYRAD package methods.

Fig. 6

(a)



(b)

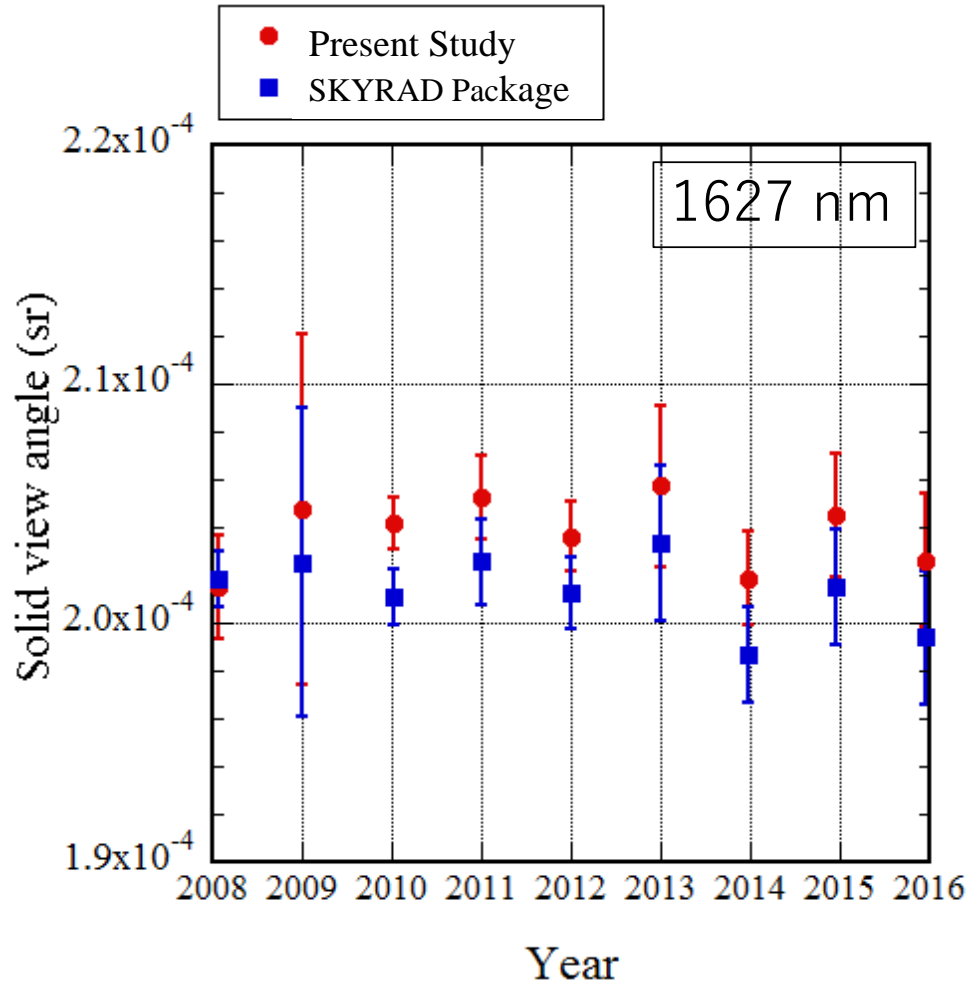


Fig.6 Same as Fig. 5 but for the [shortwave-infrared](#) region (InGaAs photodiode). The wavelength in (b) is 1627 nm.

Fig. 7

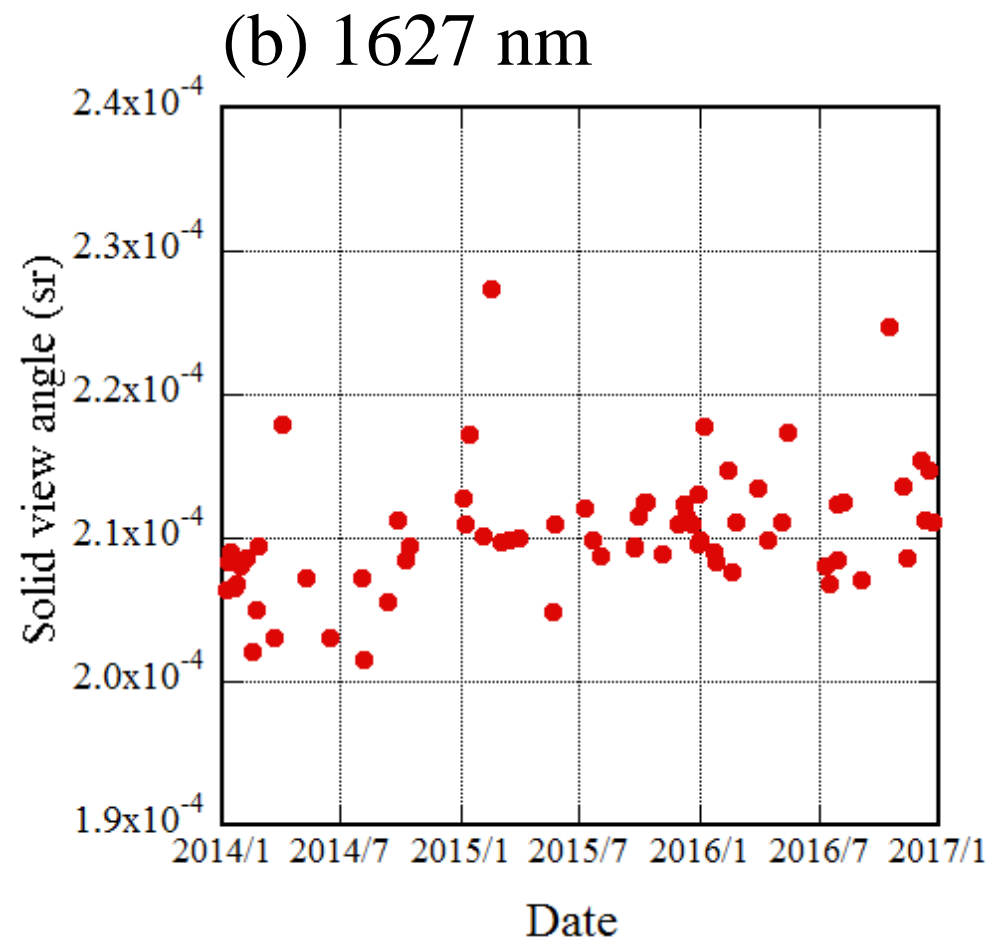
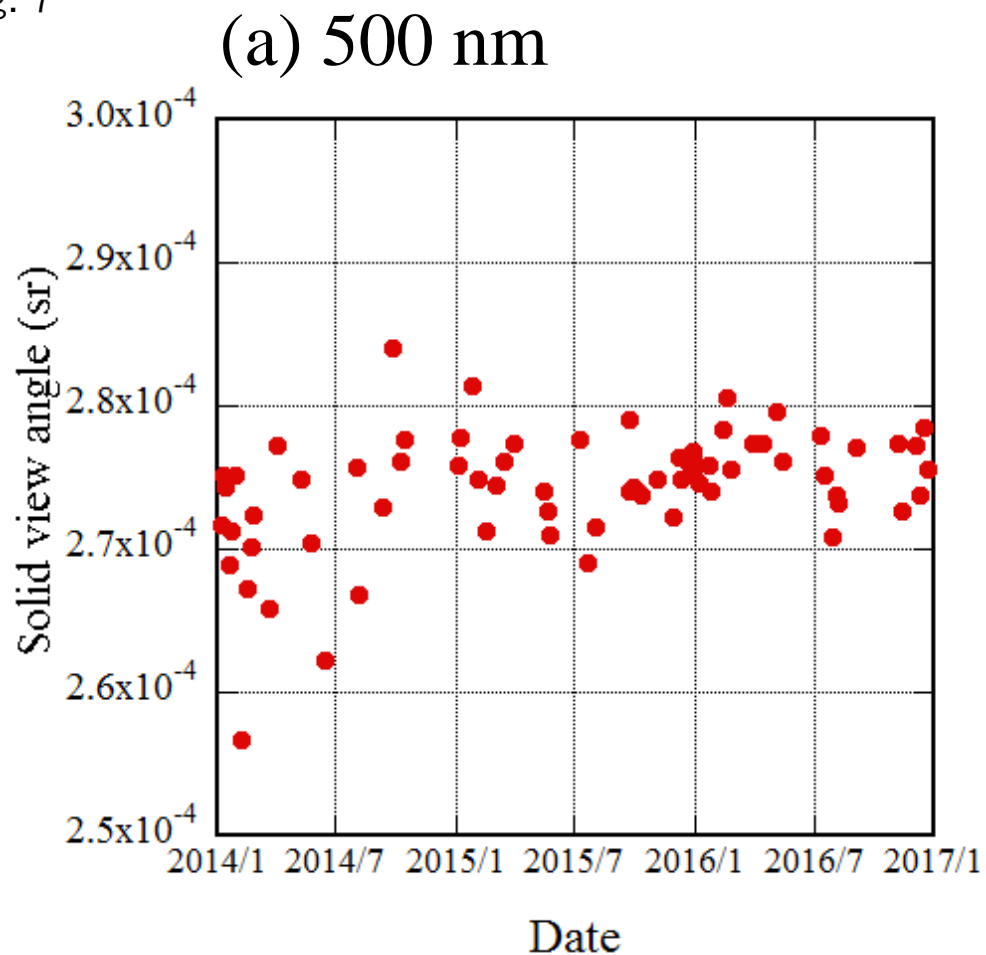


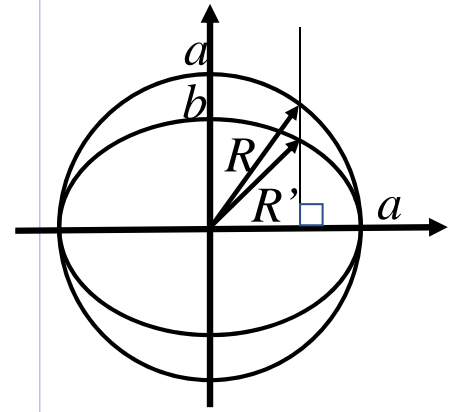
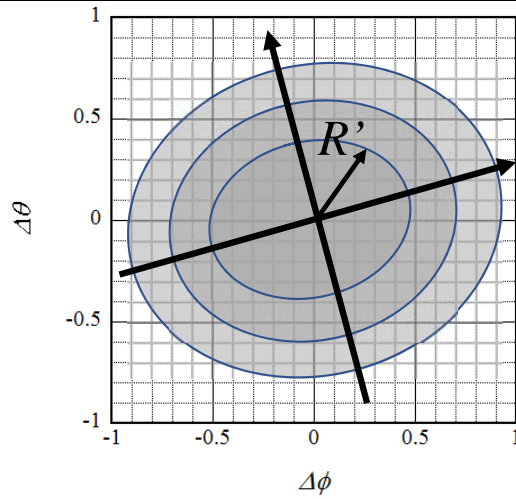
Fig.7 Time series of SVA of POM-02(Tsukuba) in the period from January 2014 to December 2016, (a) 500nm, Mean value and standard deviation are 2.743×10^{-4} and 4.2×10^{-6} , (b) 1627nm, Mean value and standard deviation are 2.104×10^{-4} and 4.4×10^{-6} , respectively.

Fig. C1

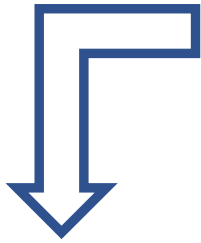
SVA calculation flowchart

(1)

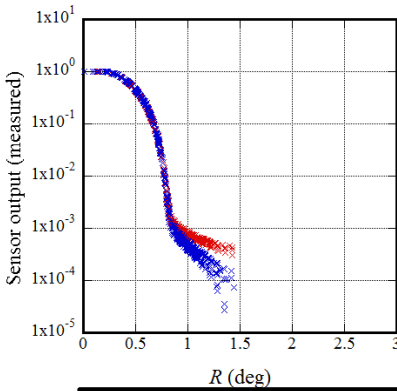
Solar Disk Scan
(21x21 grid)



- Determination of center (x_c, y_c) ($\sim(0,0)$)
- Determination of elliptic parameters
direction of major axis of the ellipse
ratio of minor axis to major axis ($b/a < 1$)
- Conversion of distance from R' to R
 $R'_{max} \sim 1\text{deg} \times \sqrt{2} = 1.41\text{ deg}$
- In the SKYRAD package, the min. value is subtracted from the measured values.

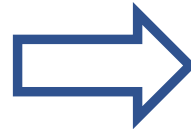


(2)

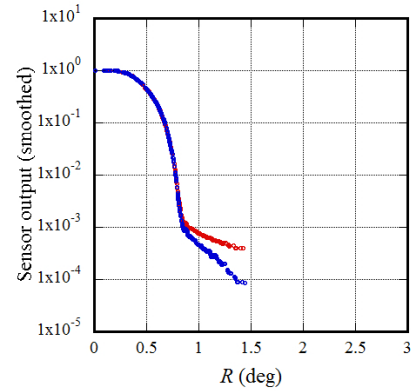


Measured values

(3)

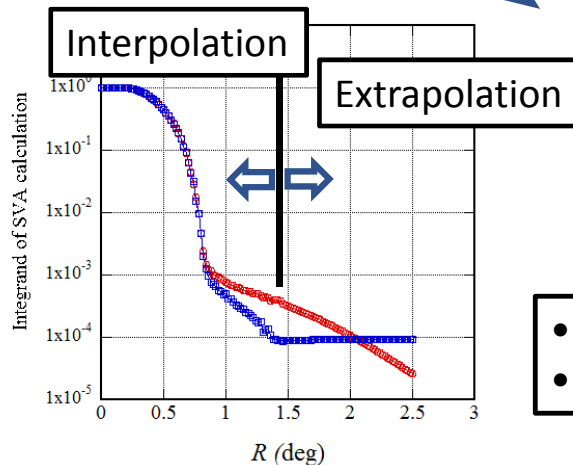


Smoothing



Smoothed values

(4)



- Integration
- Correction of ellipse

